Organometal Halide Perovskite Artificial Synapses

*Wentao Xu, Himchan Cho, Young-Hoon Kim, Young-Tae Kim, Christoph Wolf, Chan-Gyung Park, and Tae-Woo Lee**

A human brain is a high-density neural network composed of ≈10^{12} neurons and ≈10^{15} synapses; it occupies less than 2 L space and consumes less power than a household incandescent bulb, but can outperform supercomputers in many tasks.[1,2] To construct an artificial intelligent system that has these merits of a natural neural network,[3] a key step is to design an artificial synapse that emulates essential synaptic functions in a single electronic device, and consumes only femtojoule-level amounts of energy. To achieve these goals, several types of electronic devices have been developed based on resistive switchable memory,[4] phase change memory,[5] atomic switches,[6] ferroelectric tunnel junctions,[7] and synaptic transistors.[8] However, to achieve the small feature size, ultralow energy consumption, and working principles of biological synapses, new materials and electronic devices are still required.

Organometal halide perovskites (OHPs) constitute a family of materials that have recently been used to boost the power conversion efficiency of solar cells.[9] OHPs have many superior properties, such as long charge-carrier diffusion length, strong light absorptivity, ambipolar charge transport, high open-circuit voltage, and solution processibility, and therefore have broad applications such as photovoltaics,[10,11] light-emitting diodes,[12] transistors,[13] and photon-detectors.[14] OHP-based electronic devices usually exhibit significant hysteresis,[15] which may originate from ferroelectricity, charge-carrier traps, and migration of ions.[16] Those mechanisms would be valuable properties for an artificial synapse, which require gradual modulation of responses.

Herein, we fabricate and characterize an artificial synapse made from a bromine-containing OHP, $CH_3NH_3PbBr_3$. This work represents the first attempt to apply OHP to an artificial synapse. The artificial synapse emulates important synaptic characteristics in a single electronic device, including excitatory postsynaptic current (EPSC), paired-pulse facilitation (PPF), short-term potentiation (STP), long-term potentiation (LTP), and spike-timing dependent plasticity (STDP).

Artificial synapses in a two-terminal structure of substrate/buffer-capped conducting polymer (BCCP) electrode/OHP/top electrode were fabricated to emulate important working principles of biological synapses (**Figure 1**). Metal-dot top electrodes emulate the presynaptic membrane at which presynaptic spikes are applied. Electrical pulses that are analogous to presynaptic spikes are applied to the top electrodes to induce ion migration in the OHP matrix to modulate the conductance of the thin film. Conductive paths form in the ion-rich OHP matrix to provide paths for ion migration and charge-carrier transportation; these emulate the synaptic cleft that allows transmission of neurotransmitters. The BCCP thin film and the conductive sublayer (indium tin oxide (ITO)-coated glass or highly doped silicon wafer (n+Si)) together work as a bottom electrode, which emulate the functions of the dendrites of a postneuron to receive transient signals through the synaptic connection. BCCP consists of poly(3,4-ethylenedioxythiophene):poly(styrene sulfonate) (PEDOT:PSS) (Clevios P VP AI4083) and a perfluorinated ionomer, tetrafluoroethylene-perfluoro-3,6-dioxa-4-methyl-7-octenesulfonic acid copolymer (PFI) (PEDOT:PSS:PFI = 1:2.5:11.2 (w:w:w)).[17] The conductance of OHP can be temporarily or persistently tuned by pulse-induced ion redistribution across the thin film, or ion injection into the BCCP layer to leave more vacancies. The BCCP layer could serve as a reservoir to trap mobile ions. These processes consecutively modulate the conductance of OHP thin film to realize multilevel state memory and thereby emulate the tunable synaptic response of natural systems.

All of the thin films showed full coverage on the substrate (**Figure 2**a–d and Figure S1 (Supporting Information)). A 40% solution produced a thin film that was composed of grains with diameters from 200 nm to 1 μm and had a relatively rough surface (Figure 2a and Figure S2a (Supporting Information)) with root-mean-square (RMS) roughness of 22.5 nm (Figure 2b). A 20% solution yielded a smoother surface with no obvious separate grains (Figure 2c and Figure S2b (Supporting Information)), and RMS roughness of 8.84 nm (Figure 2d). Out-of-plane X-ray diffraction (XRD) patterns (Figure 2e,f) of the relatively thick film reveal a polycrystalline OHP with variable orientations (Figure 2e),[18] which implies that the lattice has a cubic structure. On the relatively thin film (Figure 2f), the peaks (100), (200), and (300) were very clean; this observation indicates that the orientation of crystallites was uniform. This uniformity might be a result of the favorably oriented crystal growth on the underlying BCCP surface. When the film is relatively thin, the interfacial effect is obvious during crystallite-formation processes. When the film is relatively thick, the interfacial effect still occurs, but it has relatively weak effect on the upper layers of crystallites.

Current–voltage (*I*–*V*) switching behavior of the artificial synapse was characterized by connecting a metal probe to the top electrode to supply voltage sweeps while the bottom electrode was grounded (**Figure 3**). Incremental increase in current was achieved by consecutively increasing the step voltages

Prof. Dr. W. Xu, H. Cho, Y.-H. Kim, Y.-T. Kim, C. Wolf, Prof. Dr. C.-G. Park, Prof. Dr. T.-W. Lee
Department of Materials Science and Engineering
Pohang University of Science and Technology (POSTECH)
Pohang, Gyungbuk 790-784, Republic of Korea
E-mail: twlee@postech.ac.kr, taewlees@gmail.com

DOI: 10.1002/adma.201506363

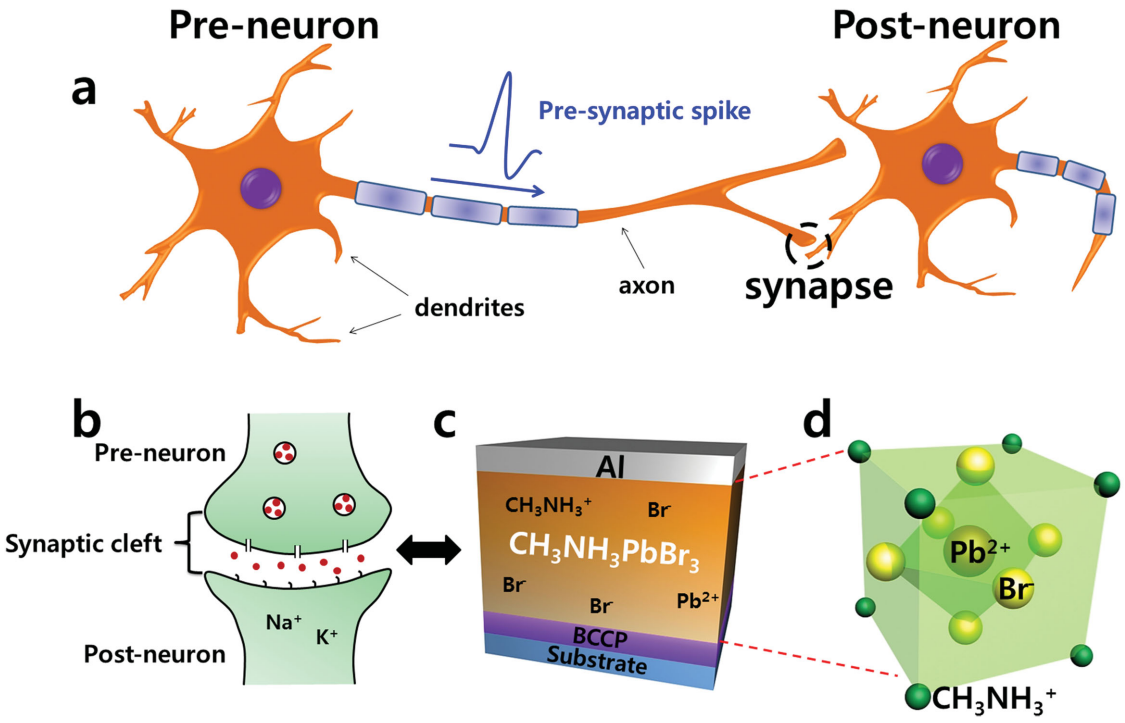

Figure 1. Schematic demonstrations of a) correlated neurons and their connections, i.e., synapses, b) fine structure of a synapse, including presynaptic membrane, postsynaptic membrane, and the synaptic cleft, c) geometry of an OHP perovskite artificial synapse, and d) crystal structure of $CH_3NH_3PbBr_3$ and spatial distributions of $CH_3NH_3^+$ (green), Pb^{2+} (pink), and Br^- (yellow).

(−2, −3, −4, −5, −6 V) in a process that emulates memristive SET processes with multilevel resistance states. No further increase in current was observed in response to further voltage sweep between 0 and −7 V. Positive sweep loops were then applied to RESET the resistance states. Both the SET and RESET showed gradual changes in current level; such changes are essential for artificial synapse applications to provide a number of consecutively variable synaptic strengths. *I–V* hysteresis behavior with respect to the scan direction in OHP-based photovoltaic devices was previously reported.[10,19] The origin of the hysteresis is still under debate; it might originate from migration of ions, ferroelectricity of OHP, or the presence of charge-carrier traps.

Synaptic plasticity is a change in synaptic weight in response to stimuli, and is believed to underlie computation and memory in a brain.[2] Synaptic weight, i.e., the strength of synaptic connection, is usually indicated by the postsynapse potential or current. In a real neuron, an action potential arrives at the presynaptic membrane to cause influx of Ca^{2+}, which initiates the release of neurotransmitters, and thereby temporarily enhance synaptic transition.[20] Our artificial synapse emulates important functions of a biological synapse. The electrical pulses applied to the top electrode are analogous to presynaptic spikes onto the presynaptic membrane (**Figure 4**a). A continuous voltage bias was applied on the bottom electrode as a reading voltage, which is small enough (0.1 V) to minimize its effect on device conductance. The postsynaptic current level increased abruptly after the pulse, then decayed rapidly over time; this change in electrical response is analogous to EPSC, which is a measure of synaptic weight (Figure 4b). The decay of postsynaptic current was due to the change in electronic conductance of the OHP thin film which is caused by back-diffusion of ions after the pulse was removed (Figure S3, Supporting Information).[21] Presynaptic spikes were used to trigger EPSCs 100 times; the EPSCs did not show obvious change in current level (standard deviation <1%); this result means that the response is stable and reproducible. The time constant (τ_{RC}) of resistance-capacitance (RC) delay is calculated to be 6.67×10^{-7} s (Figure S4, Supporting Information), which is several orders of magnitudes lower than τ_{EPSC} (93 ms); this difference eliminates the possibility that RC delay is a main cause of EPSC. Charge traps induced by bromide vacancies are shallow in or near the conduction band of OHP, and thus the charge trapping effects of these traps are not considered.[22]

STP is a temporal modification of synaptic strength, which then quickly returns to its initial state in hundreds to thousands of milliseconds if synaptic activity is not continued. STP is involved in important brain functions such as pattern recognition, associative learning, and sound localization.[23,24] One of the most well-known STP is PPF,[25] by which synaptic strength is temporally increased by an impulse if it closely follows a prior one. In a biological synapse, this strengthening is usually caused by an increase in presynaptic Ca^{2+} concentration, which results in an increase in the quantity of neurotransmitters released at the synapse. Analogously, synaptic weight in the artificial synapse was increased when a pair of successive stimuli was applied (Figure 4c). The synaptic enhancement correlates with the time interval Δt_{pre} between presynaptic spikes (Figure 4d). The synaptic enhancement slowly decayed as Δt_{pre} was increased. Spike-duration-dependent plasticity was observed (**Figure 5**a). When spiking amplitude was fixed, EPSC increased as the spiking time was increased.

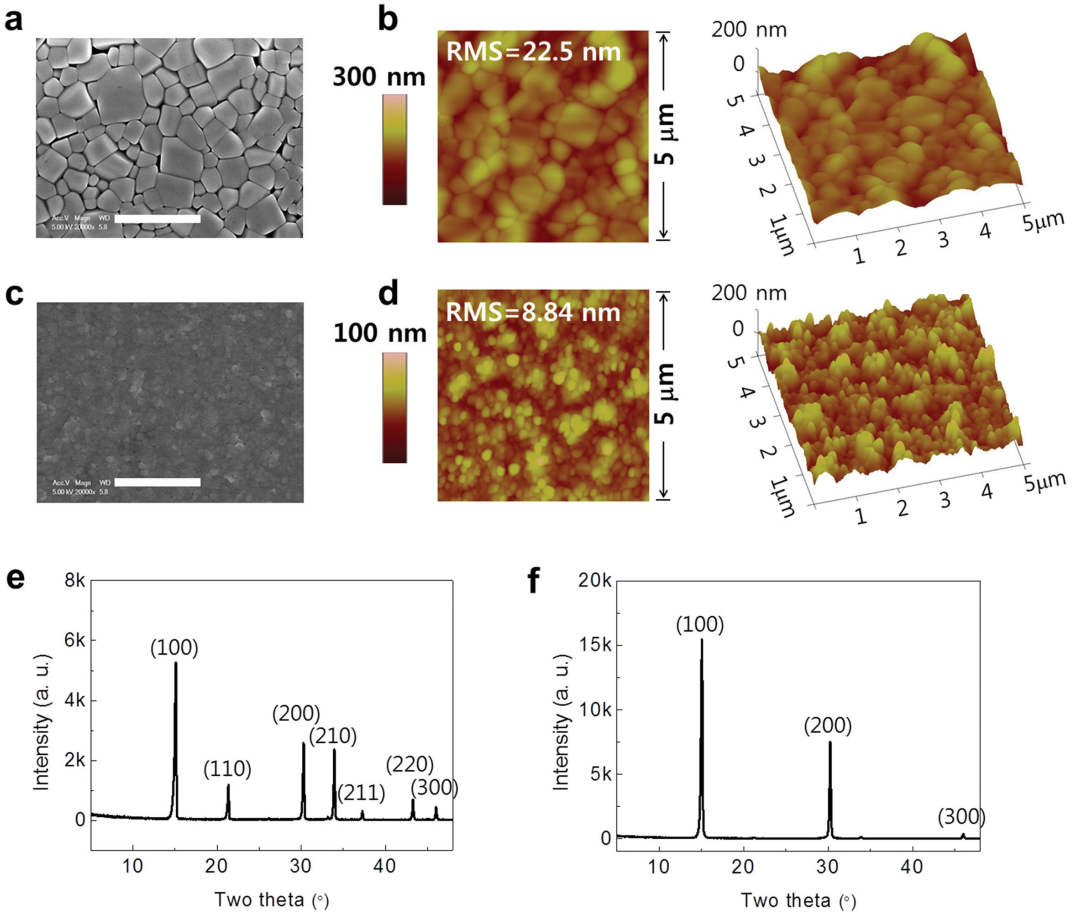

Figure 2. a) SEM and b) AFM images of 40%-solution-produced OHP thin film (SEM scale bar: 2μm). c) SEM and d) AFM images of OHP thin film produced using 20% solution. XRD patterns of OHP thin film produced using e) 40% solution and f) 20% solution.

LTP[26] is a persistent strengthening of synaptic connections based on recent patterns of activity. These patterns of synaptic activity produce a long-lasting increase in signal transmission between two neurons. In biological synapses, the increase in synaptic strength is usually caused by the release of neurotransmitters.[27] Application of a number of presynaptic spikes in a short period triggered a much increased current level, and although it decayed over time, it stabilized at a level and did not decay further for an extended time (Figure 5b). This result is consistent with biological long-term memory. The synaptic enhancement was measured to be ≈70% compared to the resting current level; this result is an evidence that long-term potentiation was realized in the artificial synapse.

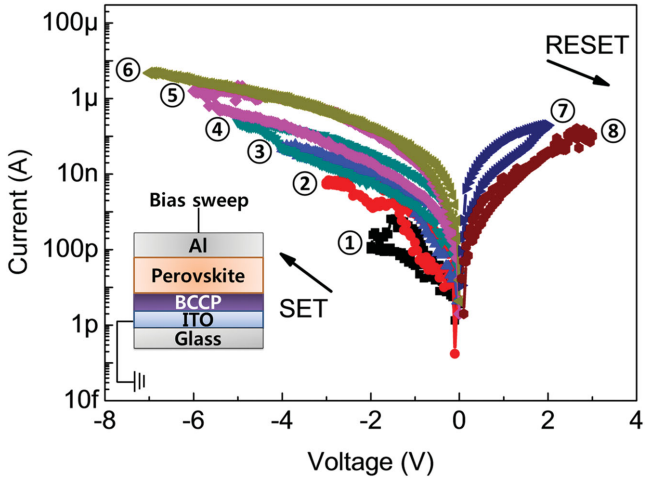

Figure 3. DC *I–V* sweeps with consecutively increased ranges that induced gradual setting and resetting processes. Inset: Schematic of the architecture and measurement of the OHP-thin-film based artificial synapse.

STP and LTP of a perovskite synapse may be caused by consecutive enhancement in conductance due to the increased number of halide vacancy defects in OHP as a result of bromide migration in response to external electrical pulses (Figure 5c). This is consistent with previous reports regarding perovskite oxides and halides. Many perovskite oxides have conductivity mediated by oxygen defects,[28,29] and low activation energy E_a of halide migration causes tunable conductivity in perovskite halides (i.e., $CuPbI_3$, $CsPbCl_3$).[30–32] It was recently found that OHP has severe halide migration under external electrical fields.[33–35]

In a perovskite synapse, the conductivity may be a result of the ion vacancy defects (green, Figure 5c). Electrical pulses drive migration of ions. When the pulse amplitude is low and

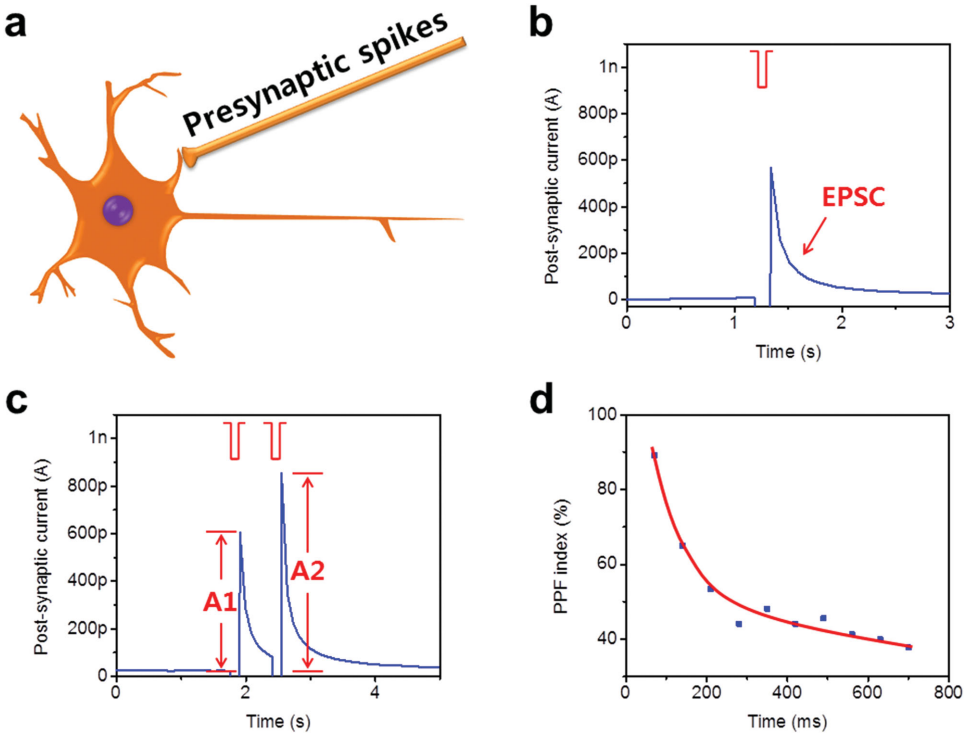

Figure 4. a) Schematic of application of presynaptic spikes through a synapse for the transmission of a signal to a second neuron. b) EPSC triggered by an applied external pulse. c) Synaptic enhancement achieved by two successively applied pulses, emulating a biological process of PPF. d) PPF index versus time interval between successive pulses.

the pulse number is small, some ions just move in a short distance then quickly return to their positions. This process causes conductance to increase sharply, and then decay quickly, which underlies the mechanism of short-term plasticity (e.g., PPF). The ionic migration that causes redistribution of ions (p-i-n homojunction) across the OHP thin film is beneficial to memristive behaviors.[21]

When a strong pulse or numerous pulses are applied, a fraction of ions can travel far enough to be trapped at the OHP/BCCP interface or even be injected into the BCCP and become trapped there. After the pulses, some ions drift back to their equilibrium positions, but some remain trapped at the interface and in the BCCP; consequently some of the halide sites in the OHP are vacant to form conductive paths. The increase in conductance can be maintained for much longer time. Therefore, after the pulses, EPSC first decays due to drifting back of partial anions, but then the current level after this decay maintained for long time, due to the increased number of defect sites. This process emulates the long-term potentiation in human memory. The penetration of ions could be observed in energy dispersive spectroscopy (EDS) mapping of transmission electron microscope (TEM) images near the interface (Figure 5d,e). Due to the relatively low E_a of Br^- (≈0.2 eV), it migrates easily under external pulses. Even though MA^+ ions have much larger E_a (≈0.8 eV) than Br^-, their possible migration cannot be fully excluded so that they might also contribute to this mechanism.[36] Although OHP synapse with a 40% solution-coated OHP thin film has more grain boundaries to facilitate ion migration, it is not as sensitive as the one with a 20% solution-coated thin film in response to the same stimulus, due to the much thicker OHP thin film (Figure S5, Supporting Information).

STDP is an asymmetric form of Hebbian learning, in which the synaptic strength can be adjusted by the relative timing of presynaptic and postsynaptic spikes. STDP is essential in neural computation; the OHP synapse emulated this behavior (Figure S6, Supporting Information). Spiking-rate-dependent plasticity was also found applicable to the device (Figure S7, Supporting Information). Presynaptic spikes of various amplitude were applied to trigger postsynaptic currents to estimate the minimum energy consumption of the artificial synapse (Figure S8, Supporting Information). Energy consumption was calculated by multiplying the pulse amplitude A, postsynaptic current I, and pulse duration t.[37] The minimal energy consumption as low as ~20 fJ per synaptic event was achieved. This value is very low among currently available synapse-emulating electronic devices. This ultralow energy consumption is a result of the abundance of ions with low E_a that can easily migrate along grain boundaries in $MAPbBr_3$ thin film, and thereby make the OHP synapse very sensitive to external stimuli even down to tens of millivolts. These results imply that the perovskite artificial synapses have great potential for use in neuromorphic electronic systems that achieve the low energy consumption of a natural neural network.

In conclusion, we fabricated and characterized a hybrid-halide perovskite synapse that emulates excitatory postsynaptic current, PPF, STP, LTP, and STDP of a biological synapse. These characteristics were realized by the consecutive

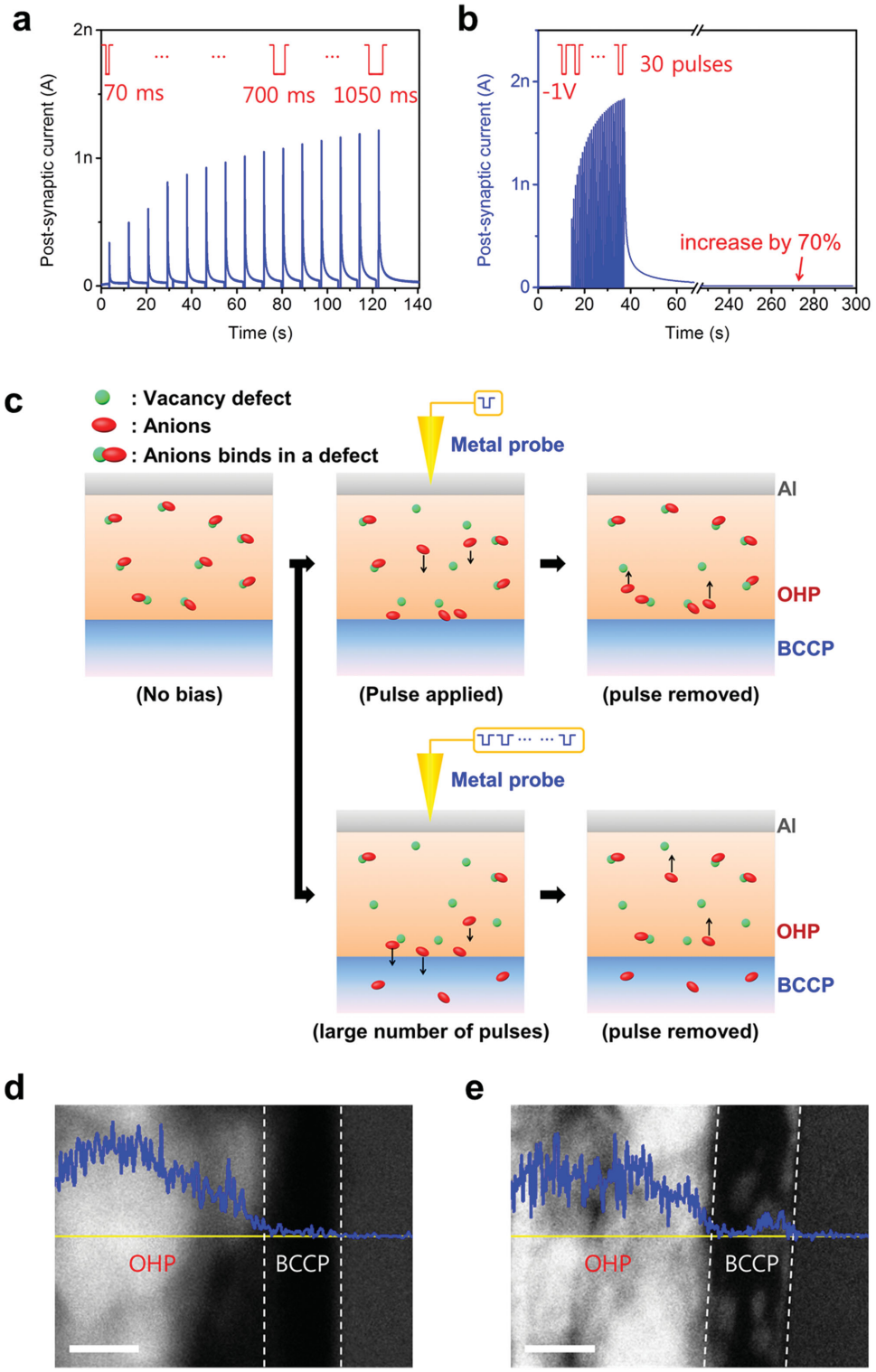

Figure 5. a) Postsynaptic current in the artificial synapse as a function duration and amplitude of presynaptic spike. b) Long-term potentiation achieved by application of a number of consecutive pulses to the artificial synapse. c) Schematic demonstration of the correlated change in the artificial synapse with the formation of short-term memory and long-term memory. TEM images and Br EDS profiles of the cross-section of OHP/BCCP structure d) before and e) after applying a series of pulses to form LTP (yellow line: position EDS line profile; blue line: intensity of Br element; scale bar: 20 nm).

modulation of electronic conductance that is a result of ionic migration mechanism in the organometal halide perovskite thin film. This is the first organic–inorganic hybrid perovskite artificial synapse. These properties present new resources for development of neuromorphic electronics.

Experimental Section

Materials Synthesis: CH_3NH_3Br solution was prepared by reacting 50 mL of hydrobromic acid (48% in water, Aldrich) and 30 mL of methylamine (40% in methanol, Junsei Chemical Co. Ltd.) in a 250-mL round-bottom flask at 0 °C for 2 h while stirring. The solvent was evaporated at 50 °C for 1 h to leave white precipitate, which was purified by recrystallization using ethanol and diethyl ether, and then dried at room temperature under vacuum for 24 h. Then 40 wt% or 20% $CH_3NH_3PbBr_3$ solution in N,N-dimethylformamide (DMF) was prepared by reacting equimolar CH_3NH_3Br and $PbBr_2$ (Aldrich) at 60 °C for 30 min.

Device Fabrication: Conductive substrates (ITO-coated glass or n+Si) were cleaned by sonication in acetone and 2-propanol, boiled in 2-propanol, dried, and treated with UV-ozone. BCCP was composed of PEDOT:PSS (Clevios P VP AI4083) and a perfluorinated ionomer, PFI (PEDOT:PSS:PFI = 1:2.5:11.2 (w:w:w)). A small amount of dimethyl sulfoxide (DMSO) additive was added to the composition to increase the conductivity. BCCP was spin-coated to form a thin film, then baked at 150 °C for 30 min. $CH_3NH_3PbBr_3$ was then spin-coated on the BCCP thin layer, and the combination was baked at 90 °C for 10 min. Then 100-nm-thick circular Al metal dots were thermally evaporated through a shadow mask in a high-vacuum chamber ($<10^{-6}$ Torr).

Measurements: Scanning electron microscopy (SEM) imaging was performed on a JEOL-6500 field-emission microscope. Atomic force microscopy (AFM) images were obtained using a Dimension 3100 microscope (Digital Instruments). High-resolution TEM with EDS was obtained using a TEM (JEOL JEM-2100FS). All electrical characteristics of the electronic devices were measured in a nitrogen-filled glove box using a Keithley 4200-SCS semiconductor parameter analyzer.

Supporting Information

Supporting Information is available from the Wiley Online Library or from the author.

Acknowledgements

W.X. would like to acknowledge Dr. Lihai Wang and Dr. Zuoli He for fruitful discussions and helpful comments and Hyeong Han for wiring the samples. This research was supported by the Pioneer Research Center Program through the National Research Foundation (NRF) of Korea funded by the Ministry of Science, ICT and Future Planning (2012-0009460).

Received: December 22, 2015
Revised: April 17, 2016
Published online: May 11, 2016

[1] V. M. Ho, J.-A. Lee, K. C. Martin, *Science* **2011**, *334*, 623.
[2] L. F. Abbot, W. G. Regehr, *Nature* **2004**, *431*, 796.
[3] A. Williamson, M. Ferro, P. Leleux, E. Ismailova, A. Kaszas, T. Doublet, P. Quilichini, J. Rivnay, B. Rózsa, G. Katona, C. Bernard, G. G. Malliaras, *Adv. Mater.* **2015**, *27*, 4405.
[4] S. H. Jo, T. Chang, I. Ebong, B. B. Bhadviya, P. Mazumder, W. Lu, *Nano Lett.* **2010**, *10*, 1297.
[5] D. Kuzum, R. G. D. Jeyasingh, B. Lee, H.-S. P. Wong, *Nano Lett.* **2012**, *12*, 2179.
[6] T. Hasegawa, T. Ohno, K. Terabe, T. Tsuruoka, T. Nakayama, J. K. Gimzewski, M. Aono, *Adv. Mater.* **2010**, *22*, 1831.
[7] A. Chanthbouala, V. Garcia, R. O. Cherifi, K. Bouzehouane, S. Fusil, X. Moya, S. Xavier, H. Yamada, C. Deranlot, N. D. Mathur, M. Bibes, A. Barthélémy, J. Grollier, *Nat. Mater.* **2012**, *11*, 860.
[8] a) A. M. Shen, C.-L. Chen, K. Kim, B. Cho, A. Tudor, Y. Chen, *ACS Nano* **2013**, *7*, 6117; b) F. Alibart, S. Pleutin, D. Guérin, C. Novembre, S. Lenfant, K. Lmimouni, C. Gamrat, D. Vuillaume, *Adv. Funct. Mater.* **2010**, *20*, 330; c) C. J. Wan, L. Q. Zhu, Y. H. Liu, P. Feng, Z. P. Liu, H. L. Cao, P. Xiao, Y. Shi, Q. Wan, *Adv. Mater.* **2016**, DOI: 10.1002/adma.201505898; d) Y. H. Liu, L. Q. Zhu, P. Feng, Y. Shi, Q. Wan, *Adv. Mater.* **2015**, *27*, 5599; e) L. Q. Zhu, C. J. Wan, L. Q. Guo, Y. Shi, Q. Wan, *Nat. Commun.* **2014**, *5*, 3158.
[9] A. Kojima, K. Teshima, Y. Shirai, T. Miyasaka, *J. Am. Chem. Soc.* **2009**, *131*, 6050.
[10] J. H. Heo, D. H. Song, H. J. Han, S. Y. Kim, J. H. Kim, D. Kim, H. W. Shin, T. K Ahn, C. Wolf, T.-W. Lee, S. H. Im, *Adv. Mater.* **2015**, *27*, 3424.
[11] N. J. Jeon, J. H. Noh, Y. C. Kim, W. S. Yang, S. Ryu, S. I. Seok, *Nat. Mater.* **2014**, *13*, 897.
[12] a) H. Cho, S.-H. Jeong, M.-H. Park, Y.-H. Kim, C. Wolf, C.-L. Lee, J. H. Heo, A. Sadhanala, N. S. Myoung, S. Yoo, S. H. Im, R. H. Friend, T.-W. Lee, *Science* **2015**, *350*, 1222; b) Y.-H. Kim, H. Cho, J. H. Heo, T.-S. Kim, N. Myoung, C.-L. Lee, S. H. Im, T.-W. Lee, *Adv. Mater.* **2015**, *27*, 1248; c) Z.-K. Tan, R. S. Moghaddam, M. L. Lai, P. Docampo, R. Higler, F. Deschler, M. Price, A. Sadhanala, L. M. Pazos, D. Credgington, F. Hanusch, T. Bein, H. J. Snaith, R. H. Friend, *Nat. Nanotechnol.* **2014**, *9*, 687; d) G. Li, Z.-K. Tan, D. Di, M. L. Lai, L. Jiang, J. H.-W. Lim, R. H. Friend, N. C. Greenham, *Nano Lett.* **2015**, *15*, 2640; e) J. Wang, N. Wang, Y. Jin, J. Si, Z.-K. Tan, H. Du, L. Cheng, X. Dai, S. Bai, H. He, Z. Ye, M. L. Lai, R. H. Friend, W. Huang, *Adv. Mater.* **2015**, *27*, 2311.
[13] a) Y. Mei, C. Zhang, Z. V. Vardeny, O. D. Jurchescu, *MRS Commun.* **2015**, *5*, 297; b) X. Y. Chin, D. Cortecchia, J. Yin, A. Bruno, C. Soci, *Nat. Commun.* **2015**, *6*, 7383.
[14] a) L. Dou, Y. Yang, J. You, Z. Hong, W.-H. Chang, G. Li, Y. Yang, *Nat. Commun.* **2014**, *5*, 5404; b) Y. Lee, J. Kwon, E. Hwang, C.-H. Ra, W. J. Yoo, J.-H. Ahn, J. H. Park, J. H. Cho, *Adv. Mater.* **2015**, *27*, 41.
[15] a) H.-S. Kim, I. Mora-Sero, V. Gonzalez-Pedro, F. Fabregat-Santiago, E. J. Juarez-Perez, N.-G. Park, J. Bisquert, *Nat. Commun.* **2013**, *4*, 2242; b) J. M. Frost, K. T. Butler, F. Brivio, C. H. Hendon, M. van Schilfgaarde, A. Walsh, *Nano Lett.* **2014**, *14*, 2584.
[16] H. J. Snaith, A. Abate, J. M. Ball, G. E. Eperon, T. Leijtens, N. K. Noel, S. D. Stranks, J. T.-W. Wang, K. Wojciechowski, W. Zhang, *J. Phys. Chem. Lett.* **2014**, *5*, 1511.
[17] a) T.-W. Lee, Y. Chung, O. Kwon, J.-J. Park, *Adv. Funct. Mater.* **2007**, *17*, 390; b) T.-H. Han, Y. Lee, M.-R. Choi, S.-H. Woo, S.-H. Bae, B. H. Hong, J.-H. Ahn, T.-W. Lee, *Nat. Photonics* **2012**, *6*, 105; c) T.-H. Han, M.-R. Choi, S.-H. Woo, S.-Y. Min, C.-L. Lee, T.-W. Lee, *Adv. Mater.* **2012**, *24*, 1487; d) K.-G. Lim, H.-B. Kim, J. Jeong, H. Kim, J. Y. Kim, T.-W. Lee, *Adv. Mater.* **2014**, *26*, 6461; e) M.-R. Choi, T.-H. Han, K.-G. Lim, S.-H. Woo, D. H. Huh, T.-W. Lee, *Angew. Chem. Int. Ed.* **2011**, *50*, 6274.
[18] J. Shi, S. D. Ha, Y. Zhou, F. Schoofs, S. Ramanathan, *Nat. Commun.* **2013**, *4*, 2676.
[19] Y. Shao, Z. Xiao, C. Bi, Y. Yuan, J. Huang, *Nat. Commun.* **2014**, *5*, 5784.
[20] T. Chang, S.-H. Jo, W. Lu, *ACS Nano* **2011**, *5*, 7669.

[21] Z. Xiao, Y. Yuan, Y. Shao, Q. Wang, Q. Dong, C. Bi, P. Sharma, A. Gruverman, J. Huang, *Nat. Mater.* **2015**, *14*, 193.
[22] T. Shi, W.-J. Yin, F. Hong, K. Zhu, Y. Yan, *Appl. Phys. Lett.* **2015**, *106*, 103902.
[23] a) P. A. Merolla, J. V. Arthur, R. Alvarez-Icaza, A. S. Cassidy, J. Sawada, F. Akopyan, B. L. Jackson, N. Imam, C. Guo, Y. Nakamura, B. Brezzo, I. Vo, S. K. Esser, R. Appuswamy, B. Taba, A. Amir, M. D. Flickner, W. P. Risk, R. Manohar, D. S. Modha, *Science* **2014**, *345*, 668; b) R. S. Zucker, W. G. Regehr, *Annu. Rev. Physiol.* **2002**, *64*, 355; c) E. S. Fortune, G. J. Rose, *Trends Neurosci.* **2001**, *24*, 381.
[24] L. F. Abbot, W. G. Regehr, *Nature* **2004**, *431*, 796.
[25] P. P. Atluri, W. G. Regehr, *J. Neurosci.* **1996**, *16*, 5661.
[26] S. F. Cooke, T. V. P. Bliss, *Brain* **2006**, *129*, 1659.
[27] T. Ohno, T. Hasegawa, T. Tsuruoka, K. Terabe, J. K. Gimzewski, M. Aono, *Nat. Mater.* **2011**, *10*, 591.
[28] L. Malavasi, C. A. J. Fisher, M. S. Islam, *Chem. Soc. Rev.* **2010**, *39*, 4370.
[29] J. B. Goodenough, *Rep. Prog. Phys.* **2004**, *67*, 1915.
[30] J. Mizusaki, K. Arai, K. Fueki, *Solid State Ionics* **1983**, *11*, 203.
[31] R. L. Narayan, S. V. Suryanarayana, *Mater. Lett.* **1991**, *11*, 305.
[32] T. A. Kuku, *Thin Solid Films* **1998**, *325*, 246.
[33] A. Dualeh, T. Moehl, N. Tétreault, J. Teuscher, P. Gao, M. K. Nazeeruddin, M. Grätzel, *ACS Nano* **2014**, *8*, 362.
[34] C. Eames, J. M. Frost, P. R. F. Barnes, B. C. O'Regan, A. Walsh, M. S. Islam, *Nat. Commun.* **2015**, *6*, 7497.
[35] T.-Y. Yang, G. Gregori, N. Pellet, M. Grätzel, J. Maier, *Angew. Chem.* **2015**, *127*, 8016.
[36] S. Meloni, T. Moeh, W. Tress, M. Franckevicius, M. Saliba, Y. H. Lee, P. Gao, M. K. Nazeeruddin, S. M. Zakeeruddin, U. Rothlisberger, M. Graetzel, *Nat. Commun.* **2015**, *7*, 10334.
[37] D. Kuzum, S. Yu, H.-S. P. Wong, *Nanotechnology* **2013**, *24*, 382001.